Status of Aquarius/SAC-D and Aquarius Salinity Retrievals

David M. Le Vine, *Fellow, IEEE*, Emmanuel P. Dinnat, Thomas Meissner, *Senior Member, IEEE*, Simon H. Yueh, *Fellow, IEEE*, Frank J. Wentz, Sandra E. Torrusio, and G. Lagerloef

***Abstract*—Aquarius was launched in June 2011 to monitor the global salinity field in the open ocean. This radiometer/scatterometer (i.e., passive/active) instrument is part of the Aquarius/SAC-D mission, a partnership between the USA and Argentina. In general, the observatory and instruments have functioned well with mostly minor issues. Aquarius has been operating successfully since being turned on August 25, 2011. The quality of the salinity retrieval has improved continuously and is approaching the accuracy goal of 0.2 psu (monthly global RMS). The maps produced by Aquarius show the global structure and dynamic features of the salinity field and, now after 3 years of operations, data are available to give a first look at the interannual changes in sea surface salinity. An improved salinity product, Version 3.0, has been released to the public (June 2014) and includes significant refinements in the retrieval algorithm such as reduced ascending/descending differences and improved calibration. Additional data such as global maps of soil moisture and maps of RFI are also available.**

***Index Terms*—Aquarius, L-band, microwave remote sensing, ocean salinity, radiometer calibration.**

I. Introduction

AQUARIUS is the primary instrument on the Aquarius/SAC-D observatory, a partnership between the USA Space Agency, National Aeronautics and Space Administration (NASA) and the Argentine Space Agency, Comisión Nacional de Actividades Espaciales (CONAE). The Aquarius/SAC-D observatory was launched on June 10, 2011 from Vandenberg Air Force Base, California, USA. Aquarius was turned on in late August and the first salinity map was released in September 2011 see [16]. Aquarius has been producing maps of the global sea surface salinity (SSS) field continuously since then.

Aquarius differs from the other L-band instruments in space, Soil Moisture and Ocean Salinity (SMOS), and Soil Moisture Active Passive (SMAP), in that it was specifically designed to map the salinity field in the open ocean (as opposed to also measuring soil moisture). This involved some specific choices in engineering and mission design. These include adding a radar scatterometer to the radiometer (the primary instrument for measuring changes in salinity) to help correct for surface roughness, and adding a polarimetric channel to the radiometer to provide a correction for Faraday rotation [26], [44]. In addition, the orbit (sun synchronous with 6 A.M./6 P.M. equatorial crossing and 7 day exact repeat) was selected with the retrieval of salinity in mind. Specifically, Aquarius is positioned to fly on the day-night terminator with the three beams looking toward the night time side to avoid sun glint [9], and the exact repeat orbit facilitates averaging to reduce noise [22]. In addition, careful attention was paid to the design of the antenna system (an offset-fed reflector with three feed horns) to minimize sidelobes in the direction of the direct and reflected ray from the Sun. Thermal stability also received considerable attention, and a combination of active and passive thermal control was developed to keep the critical elements of the radiometer front end to within 0.1 °C. The radiometer electronics itself was the result of several years of prelaunch design research [43]. Finally, rapid sampling of the data, far in excess of that needed for Nyquist sampling of the footprint, was adopted to help mitigate radio-frequency interference (RFI). In principle, by sampling rapidly, contaminated data can be removed while leaving enough good samples to execute a successful retrieval.

These features have been working well and Aquarius is producing global maps of SSS approaching the goal of monthly maps with an accuracy 0.2 psu. The value of the measurement is also being recognized. For example, assimilation of Aquarius measurement of salinity in the NASA Goddard Earth Observing System Model (GEOS-5) has shown the potential to improve general circulation models compared to using *in situ* data alone [41]. In addition, the data are being used for other applications; for example, the Aquarius project is producing global maps of soil moisture and maps of the distribution of RFI in the L-band window at 1.413 GHz where the radiometers operate. Examples of these maps can be found at the Aquarius out-reach website: http://www. aquarius.umaine.edu.

Details of the Aquarius instrument are well documented in the literature [26], [29]. The objective of this paper is to provide an overview of the status of Aquarius/SAC-D mission with a focus on the Aquarius salinity retrieval algorithm. The status of the mission and hardware is described in Section II. Section III provides an update on the recent changes to the Aquarius salinity retrieval algorithm and Section IV presents examples and performance metrics.

Manuscript received December 25, 2014; revised March 27, 2015; accepted April 17, 2015. Date of publication June 08, 2015; date of current version January 25, 2016.

D. M. Le Vine is with the Goddard Space Flight Center, Greenbelt, MD 20771 USA.

E. P. Dinnat is with the Chapman University, Orange, CA 92866 USA, and also with NASA/GSFC, Greenbelt, MD 20771 USA.

T. Meissner and F. J. Wentz are with the Remote Sensing Systems, Santa Rosa, CA 95401 USA.

S. H. Yueh is with the Jet Propulsion Laboratory, Pasadena, CA 921109 USA.

S. E. Torrusio is with the Comision Nacional de Actividades Espaciales (CONAE), C1063ACH Buenos Aires, Argentina (e-mail: storrusio@conae.gov.ar).

G. Lagerloef is with the Earth and Space Research, Seattle, WA 98121 USA.

Color versions of one or more of the figures in this paper are available online at http://ieeexplore.ieee.org.

Digital Object Identifier 10.1109/JSTARS.2015.2427159

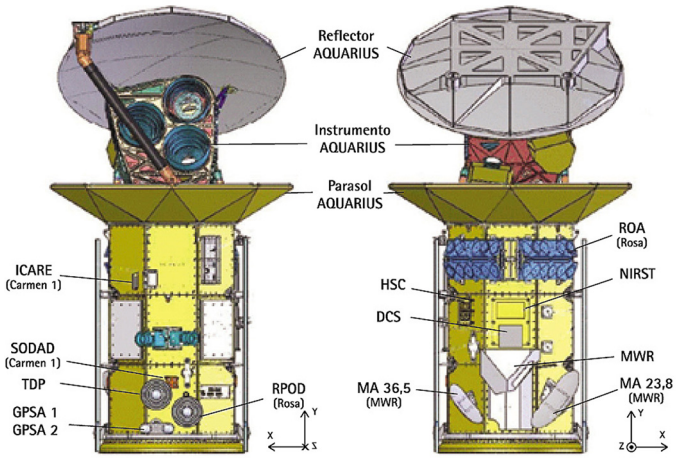

Fig. 1. Aquarius/SAC-D observatory in the stowed configuration. (*Left*) A view of the top sky-facing side of the observatory. (*Right*) A view of the bottom, Earth-facing side of the observatory. The observatory flies in the "x" direction (to the left in the left side figure) and is oriented as shown with the long axis perpendicular to the velocity vector.

Fig. 2. Photograph of the Aquarius/SAC-D observatory in the stowed configuration as it looked just prior to shipment to Vandenberg Air Force Base for launch. The silver structures to the left are Aquarius and the portion covered in gold foil is the observatory bus and associated instruments (SAC-D). The Earth viewing side is at the bottom (right inset in Fig. 1) and the sky-viewing side is at the top. (1) Aquarius reflector; (2) Aquarius sun-shield; (3) Aquarius feed horns (covered); (4) MWR antennas (stowed); (5) Cameras NIRST and HSC; (6) ROSA antennas.

II. Aquarius/SAC-D Mission

A. Overview

The Aquarius/SAC-D mission is a fully integrated partnership between NASA and CONAE. The general roles and responsibilities are illustrated in ([26], (Fig. 2)). NASA contributed the launch, which took place on June 10, 2011 aboard a Delta II launch vehicle. The Argentine space agency contributed the spacecraft bus, SAC-D, and together with partners in Italy, France and Canada, also contributed several instruments. The observatory was assembled in Bariloche, Argentina by the CONAE prime contractor, INVAP and shipped to Vandenberg AFB for launch. Once in orbit, mission control became the responsibility of CONAE. The mission is controlled through the Argentine Mission Operations Center (MOC) near Cordoba, Argentina. Data are downloaded via several ground stations including the NASA NEN, the Italian Madeira ground station and the ground station at the MOC. The data come to the MOC where it is parsed and the Aquarius data are sent to the Goddard Space Flight Center for processing. The Aquarius data products are archived at the NASA Physical Oceanography Distributed Active Archive Center (PO.DAAC) where they are also available to the public. Data from the CONAE Microwave Radiometer (MWR) is also available at the PO.DAAC. Mission operations for Aquarius (e.g., events such as cold sky calibrations) originate at the Goddard Space Flight Center and are coordinated with the CONAE Flight Operations Team and executed at the MOC. Both the NASA and CONAE teams work together to coordinate operations, downlink data, and resolve observatory issues (e.g., see "star tracker" in Section II-B).

Figs. 1 and 2 describe the observatory and instruments. Aquarius is the large structure separated from the rest of the observatory by an umbrella-like sun-shield which is part of the thermal control for Aquarius. Fig. 1 is a drawing identifying the instruments on the observatory. The view on the left is of the top (sky-facing) side of the observatory and on the right is shown the bottom (Earth-facing) side. The observatory flies to the left in the sky-facing view and is oriented as shown in the figure (i.e., with the long axis perpendicular to the velocity vector). Fig. 2 is a photograph of the actual hardware as it existed prior to shipment to Vandenberg Air Force Base for launch. The sky-facing side is toward the top of the photograph. The silver portion to the left is Aquarius shown with the reflector, 2.5 m in diameter, in the stowed configuration (1). The sun shield (2) and three feed horns (3) are also visible. The feed horns are covered in this photograph, but the covers were removed prior to launch to avoid any issues of loss associated with a radome. The observatory is oriented in the photograph as it flies in orbit, with the velocity vector perpendicular to the page and with the ground at the bottom.

The CONAE contribution to the observatory is gold colored in the photograph (Fig. 2). It includes the satellite bus and several instruments. These include the MWR, infrared and visible cameras (NIRST and HSC, respectively), an L-band radio occultation experiment (ROSA) and a space particle environment experiment (CARMEN). A description including status and results is given in Appendix A.

B. Mission Status

Overall, the Aquarius/SAC-D observatory and instruments are working well and performing within designed parameters. There is a problem with the MWR (see Appendix A) and in addition a CONAE technology demonstration package (TDP) has stopped working. However, the CONAE team feels it learned what it wanted from the TDP and no further effort will be made to recover it. The MWR is also probably lost, but all efforts to at least confirm why it failed have not ceased. Data from more than 2 years of MWR operations are available at the PO.DAAC: http://podaac.jpl.nasa.gov (also see Appendix A).

Other than these issues with the instruments, there have been two relatively minor issues with the spacecraft bus itself: 1) a problem with the star tracker which has been resolved and 2) a failure of one of the dc-to-dc converters in the power distribution network.

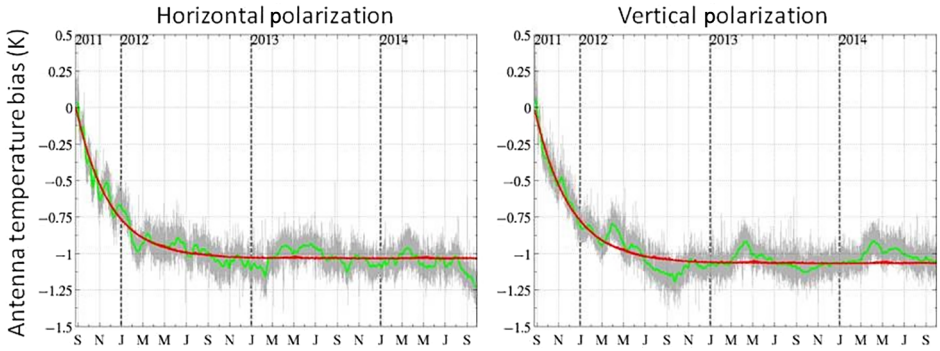

Fig. 3. Radiometer drift for the Aquarius inner beam and (*left*) horizontal polarization and (*right*) vertical polarization. (Gray) The difference between observed and expected antenna temperature for each beam and (green) 7-day average. (Red) The exponential fit used to remove the mean bias. The data are from the beginning of the mission (August 25, 2011) through September 30, 2014.

1) Star Tracker: Early in the mission the star tracker would frequently lose lock when the Moon came nearby (and also in some random situations), which caused the spacecraft to exit science mode. This was eventually corrected through a combination of modifications, which included adjusting the field of view, cooling the detector and tuning the Kalman filter in the attitude control software [29]. The backup star tracker had similar problems, with even poorer response initially, but with these changes it is now functioning near nominal. At the initial operating temperature (about 20 °C) "warm pixels" were a problem generating noise and led to a poor quality index and increasing degradation of performance. The reduction in operating temperature (now near 0 °C) appears to have corrected the problem. Both star trackers, the primary and back up, are now performing well.

2) DC–DC Converter: Power is distributed from the main source to the instruments in a tree whose branches include a redundant pair of dc-to-dc converters. About 1.5 years into the mission, one of these converters failed. The system operated as designed (i.e., the backup converter took over automatically) and there was no impact on operations. Extensive engineering analysis, including destructive testing of unused converters, has been conducted. The conclusion is that this was a random event and that it does not indicate a particular failure mode threatening the mission. The effect of this particular failure is that redundancy in one major path has been lost. However, there are many of these devices in the SAC-D hardware (they were not used by Aquarius) and a failure of a dc-dc converter is one possibility for the problems with the MWR.

C. Aquarius Instrument

Aquarius is performing well. It has been operating continuously since being turned on in August 2011 and now a history of over 3 years of global coverage of SSS in the open ocean is available for study. Details of the Aquarius instrument are well documented [26], [29]. The discussion below focuses on two radiometer issues, drift and calibration, and the status of the scatterometer.

1) Radiometer: The three Aquarius radiometers have performed very well. They are thermally stable (a change of less than 0.1 °C per orbit for the critical parts of the front end) and the observed antenna temperatures are very close to theoretical values predicted by radiative transport for the Aquarius observing geometry [28]. However, a small drift in gain has been present since launch [29]. The change is very small (about 0.24 K per month during the first months of operation when it was largest) and has gradually decreased. Although the drift might be negligible for other applications, it is significant for remote sensing of salinity where the accuracy goal is on the order of 0.1 K [23], [27].

There is evidence that at least part of this drift is attributed to the design of the back end of the radiometer and the engineering team has developed an approach for correcting at least part of the drift [36]. However, until this is fully tested, the drift is being corrected as part of the radiometer calibration.

Aquarius is calibrated by comparing the actual observation (e.g., antenna temperature) with the prediction of a forward model (computer simulation) which predicts the signal at the spacecraft and integrates over the antenna pattern [28]. The HYCOM ocean model run by U/Florida to support U.S. Navy operations [7] is used to provide the value of ocean salinity in this computation. The calibration is done on a global basis, using the global average antenna temperature. Soon after launch, this procedure was used to adjust the radiometer bias and the prelaunch estimate of the temperature of the internal reference noise diode (which is used to determine gain [38]). In the ideal case of a perfectly stable radiometer, these adjustments would have to be made only one time. However, it was clear in comparing against cold sky and stable targets like Dome-C in Antarctica, that the radiometers had a small drift.

Fig. 3 shows the drift in the case of the innermost radiometer (i.e., with the smallest incidence angle). Also, see [14], [29]. The vertical axis (ordinate) shows the difference between the observed radiometer antenna temperature and the value predicted by the forward algorithm (called "expected value" and available in the Aquarius level 2 data). This difference is plotted as a function of time since the beginning of the mission (August 25, 2011) through September 30, 2014 (3 years of observations). The data (one point per obit) are shown in gray and a 7-day average is plotted in green. The red line is an exponential fit. It also includes a constant so that the difference begins at zero at the beginning of the mission (this is the initial radiometer bias). As the figure shows, the drift has gradually stabilized,

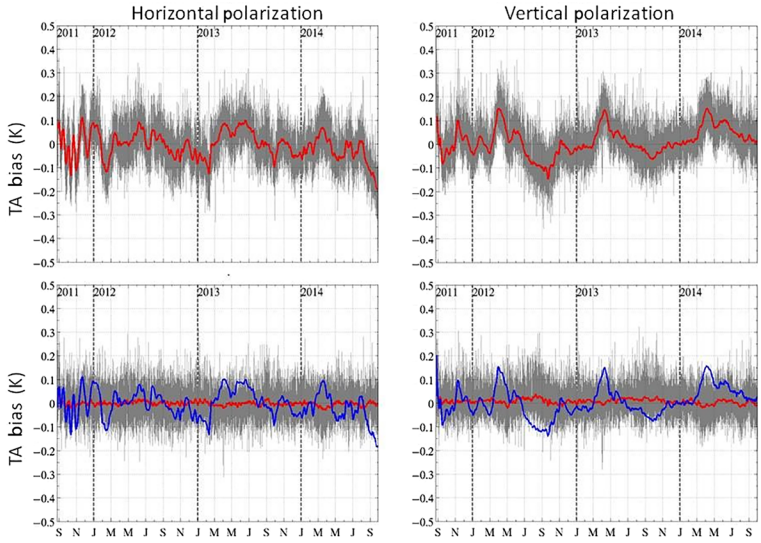

Fig. 4. Radiometer drift residual after correcting for the exponential drift for the Aquarius inner beam and (*left*) horizontal polarization and (*right*) vertical polarization for the period August 25, 2011 to September 30, 2014. (*Top*) The residual after removing the exponential (gray) averaged over 1 orbit and (red) averaged over 7-days. (*Bottom*) The corrected data after removing the 7-day average residual shown in the top panel. The blue curve is the correction, the gray curve is the corrected data, and the red curve is a 7-day average after the correction (i.e., average of the data in gray).

and after the first year the dominate feature is the oscillation about the exponential fit.

For purposes of calibration, the drift is modeled in two parts. An exponential fit to the full mission time history (red curve in Fig. 3) plus the small deviations from the exponential. The exponential is computed once by fitting a simple exponential to the radiometer history as shown in Fig. 3. The exponential is treated as an error in gain, and the gain is adjusted as a function of time to remove this portion of the drift. This is done by adjusting the noise temperature of the internal reference diode so as to cancel the exponential [38].

The residual left after removing the exponential is shown in the top panel in Fig. 4. The data (difference between observation and forward model) after removing the exponential are shown in gray and the 7-day average is shown in red. The scale has been changed (from Fig. 3) and the amplitude of the residual is on the order of ± 0.1 K. It is believed that these residuals can be traced back to issues with the radiometer hardware and that a correction can be developed which is independent of the forward algorithm [36]. However, in the meantime, they are corrected by making a second pass through the data, smoothing the residual with a sliding 7-day window. The smoothed residual is treated as a bias and removed. The lower panel in Fig. 4 shows the final product. The blue curve is the correction and the gray trace represents the corrected data. The red curve is a 7-day average of the corrected data. It is close to zero and quite stable. The data for the other two Aquarius radiometers are similar.

A complete record is kept of all the adjustments made as part of this calibration. They can be found in or can be derived from the parameters in the Aquarius level 2 data file. For a description, see the L2 Data Format Specification document for V3.0 (this is Aquarius document AQ-014-PS-0018, which is available at the PO.DAAC: http://podaac.jpl.nasa.gov). The level 2 data file also contains all of the elements of the radiative transport "forward" model used to compute the "expected" antenna temperature needed in the calibration.

The two-step procedure outlined above is the process implemented in the current Aquarius salinity retrieval algorithm (Version 3.0). Other than this small drift, the radiometers have performed well and within specifications. Their thermal stability and noise performance are within the specification (0.1 °C and a NEDT $\leq$ 0.08 K in 5.76 s, respectively).

2) Scatterometer: The scatterometer has been designed to provide a nearly simultaneous measurement of roughness over the same spot on the surface as seen by radiometer. The scatterometer and radiometers share the same antenna (feed horns and reflector) but there is only one scatterometer which sequentially cycles through the three feeds [26]. The radiometers are blanked for 1 ms during each 10 ms sample period to permit the scatterometer to transmit, and the return signals (radiometer at 1.41 GHz and scatterometer at 1.26 GHz) are isolated by large filters (frequency diplexers) to permit them to receive simultaneously. The scatterometer radar cross section is used in the salinity retrieval algorithm to correct for roughness (e.g., Section III-C3). In addition, wind speed is produced as an independent product [18].

The scatterometer has performed well since Aquarius was turned on in August 2011. The scatterometer calibration for transmit power and receiver electronics gain is accomplished by using a calibration loopback signal. That is, a small portion of the transmit signal is routed through a calibration loop into the receiver during each transmit event [26] and recorded for correcting the drift of transmit power and receiver gain in the Aquarius data processing system (ADPS). In order for this loopback technique to be effective, the losses of the calibration loop and any microwave components not enclosed by the calibration loop have to be stable. This is achieved by active temperature control. Telemetry of the temperature sensors located in the scatterometer electronics indicates that the temperature sensitive elements of the scatterometer have been controlled to within 1 °C of the expected temperature set points (which are near room temperatures).

The scatterometer transmit power and receiver gain have been very stable. The calibration loopback signal indicates a drift of about 0.15 dB in the first 6 months after turn on but changes by less than 0.05 dB after that transition period [37]. Part of this initial total change was caused by the change of receiver gain, perhaps due to outgassing or some relaxation of receiver electronics. This was determined by analyzing a part of the noise-only data imparted by the Aquarius correlated noise diode (CND) included as part of the radiometer calibration [26]. (The scatterometer alternates each transmit–receive look with a receive-only look some of which receive signal from the CND). However, part of the transient (about 0.07 dB) was caused by the transmitter or front-end components outside of the calibration loop. If the change was caused by the power of the transmitter, then there would be no impact to the calibration of the Aquarius scatterometer backscatter product because that type of change is removed by the loopback calibration. Drift outside the calibration loop has to be adjusted in the data processing [47].

A vicarious calibration technique was implemented to monitor the scatterometer calibration performance. The vicarious calibration technique computes the expected backscatter cross section (σ_0) for each Aquarius measurement using the ocean wind from the National Centers for Environmental Prediction (NCEP) and the scatterometer geophysical model function (GMF) [48]. The differences between the expected σ_0 computed this way and the σ_0 observed by Aquarius are averaged globally on a daily basis. The daily average showed a transition of about 0.06–0.08 dB in the first 6 months, which supports the CND and calibration loopback analysis [37]. Therefore, it has been concluded that there was about 0.07 dB drift (exponential-like in time) not accounted for by the calibration loopback in the first 6 months transition period. After the first 6 months, the stability of scatterometer calibration has been exceptional, about 0.05 dB (peak-to-peak) or 0.02 dB (one standard deviation) [37].

The bias in the scatterometer calibration is determined by adjusting the observations to fit those of the PALSAR GMFs for the Amazon forest and ocean [39], [48]. The initial scatterometer calibration was completed using the prelaunch measurement of the losses of the calibration loop and other front-end components. By comparison with the PALSAR GMFs for the Amazon and ocean, a 2-dB bias was introduced to adjust the Aquarius calibration. This is a relative calibration between Aquarius and PALSAR. But because PALSAR, a synthetic aperture radar, was able to use corner reflectors for absolute radiometric calibration, most of the 2-dB calibration bias should be due to the uncertainty of the prelaunch calibration data for Aquarius. However, the PALSAR GMFs for ocean and the Amazon are not entirely consistent. If one fits the Aquarius calibration bias using the PALSAR GMF for the Amazon, there will be about $\pm 0.5\,\mathrm{dB}$ bias (depending on antenna beam) with respect to the PALSAR GMF for ocean. A decision was made to use the PALSAR GMF for the Amazon for relative bias adjustment because the PALSAR GMF has all polarizations for the Amazon, but only HH-polarization for ocean.

The excellent calibration stability of Aquarius scatterometer allows the retrieval of ocean wind speed from the calibrated scatterometer σ_0 [18] and land surface soil moisture applications [40]. Fore *et al.* [18] tested the retrieval algorithms using single and dual-polarizations (HH and/or VV), and found that the dual-polarization produced the most accurate wind speed product. Direct comparison of the wind speed retrieved from the scatterometer with winds produced by SSM/I suggests a bias near zero and standard deviation on the order of 1 m/s for winds up to about 15 m/s [18].

III. Aquarius Salinity Retrieval: Version 3.0

Aquarius has been producing maps of salinity since the first image in September 2011. Data are available to the public through the NASA PO.DAAC managed at the Jet Propulsion Laboratory: http://po.daac.jpl.nasa.gov. Salinity data for the entire mission were recently reprocessed and are now available as Version 3.0. The previous version, V2.0, is obsolete and will soon be unavailable. The project team uses integers to indicate major updates (e.g., V2.0 and V3.0) which are available to the public, and the decimal (e.g., V2.1) is used to indicate evaluation products available to the science team to test changes prior to release of the product to the public. These evaluation products are maintained on the ADPS at the Goddard Space Flight Center. As of the writing of this paper, the science team is working on V3.2 and preparing to release V4.0 prior to the conclusion of the prime mission in September 2015.

The salinity retrieval algorithm is documented in the algorithm theoretical basis document, ATBD [42] plus a series of addenda which document the changes. The most recent changes are documented in Addendum III [33] and all of the documentation is available at the PO.DAAC website. Version 3.0 represents a significant change in the retrieval algorithm. The major changes are summarized below.

A. Reduction in Ascending/Descending Bias

In the ideal case, ascending and descending passes over the same ocean should yield almost the same salinity. Although differences might exist on short time-scales (e.g., due to rain), they should be insignificant for zonal averages and over time scales of weeks to months. However, small differences existed in Version 2.0. The differences were traced to the radiation from the celestial sky (galactic background radiation) reflected from the surface to the radiometer. A correction had already been made for this radiation in V2.0 using a geometrical optics model for the rough surface but it did not completely remove this signal. The residual (about 10% of the total) manifested itself as a difference between ascending and descending passes because of the different aspect angles of the radiometers on ascending and descending passes relative to the surface and sky. Since a completely theoretical correction (i.e., improved modeling of the scatter from a wind roughened surface) was not known, it was decided to remove the residual empirically and an empirical "symmetrization" of the ascending and descending passes was implemented ([33], Sec. 5).

The effect of this change is shown in Fig. 5. On the left is Hovmöller plot (latitude vs. time) showing the salinity difference between ascending and descending passes as it existed in

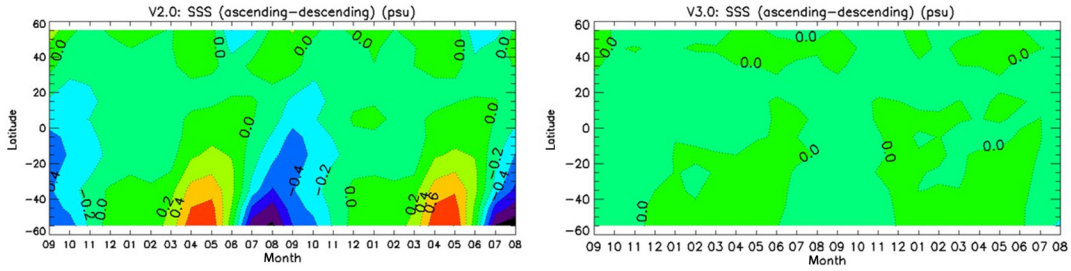

Fig. 5. Hovmöller plot of the monthly salinity difference between ascending and descending Aquarius swaths. The abscissa is time (months starting September 2011) and the ordinate is latitude. (*Left*) Using the geometric optics (GO) model for calculating the reflected galactic radiation (V2.0). (*Right*) After adding the empirical symmetrization correction (V3.0).

V2.0 using only the geometrical optics correction. On the right is the same difference as it exists in V3.0 after including the additional empirical correction.

B. Improvement in Overall Calibration

The conversion of Aquarius antenna temperature, TA, to brightness temperature, TB, is accomplished by comparing with the antenna temperature predicted by the Aquarius forward algorithm [28]. This is done in two stages [42]. First a bias is removed by comparing the global average observed TA with the predicted value. The salinity field produced by the HYCOM ocean model [7] is used in the forward algorithm for this purpose. The second step is to convert TA to TB. This is accomplished as part of a matrix inversion of the integral equation relating TA and TB called the antenna pattern correction (APC) [29], [42]. The APC corrects for imperfections in the antenna (e.g., cross-polarization coupling) and adjusts the gain of the radiometer system by accounting for the fraction of power in the Earth-viewing portion of the antenna pattern. The APC is derived empirically [42] and since the goal of Aquarius is to map SSS, the APC was tuned to the ocean.

This process works well and retrievals approaching the goal of 0.2 psu have been obtained (see Section VI-B). However, when comparing Aquarius brightness temperatures over land in V2.0 with those predicted by the forward algorithm and with those retrieved by SMOS, a significant bias was found. Differences as much as 8 K were found when comparing global means between SMOS and Aquarius over land. This is illustrated in Fig. 6 which plots the measured antenna temperature on the ordinate against the expected antenna temperature (predicted by the forward algorithm) on the abscissa. The dashed line represents agreement (1:1) and the data in this example are for horizontal polarization of the Aquarius middle beam. The red dots at the upper right are Aquarius observations over the Little River watershed and the two insets show data over ocean (upper left) and cold sky (lower right). As expected, the ocean data lie on the 1:1 curve. But the dynamic range is very small (8 K) and most of the data (red) lie within 2 K. Hence, it is possible to have a good fit even though the slope of the actual radiometer operating curve is slightly off 1:1. That the slope of the operating curve is in error can be seen by comparing the data over the Little River watershed which are too warm and the data at the cold end (insert at the lower right for cold sky) which show that the measurements at this end are too cold.

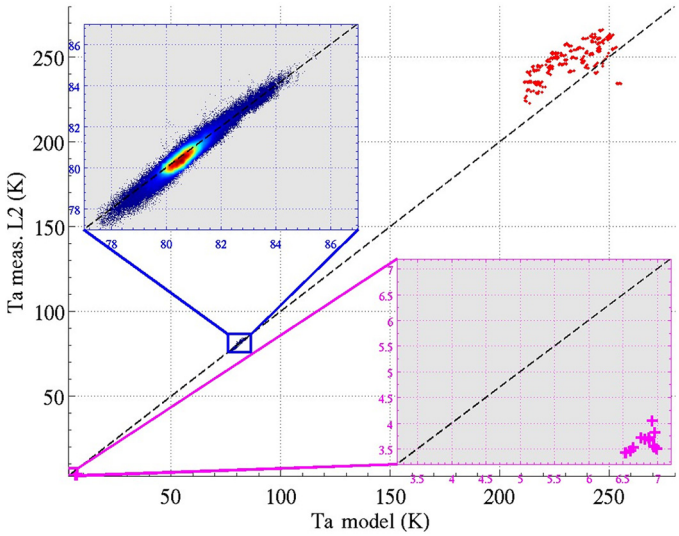

Fig. 6. Comparison of antenna temperature observed by Aquarius (ordinate) with the antenna temperature predicted by the forward model (abscissa). The insets show data over the ocean (blue) and when looking at cold sky (pink) with an expanded scale. The red dots near 250 K are data collected over the Little River research watershed in Georgia, USA.

An error in the slope of the operating curve can occur if there is an error in the antenna pattern used to derive the APC. For example, because the total antenna gain is conserved, an error in the fraction of power in the backlobes will manifest itself as an opposite error (i.e., increase or deficit) in the power in the main lobe. To confirm the suspicion that an error might exist in the characterization of the backlobes, a test was conducted to estimate the fraction of power in the backlobes. A pass was made over a well-defined land/water boundary in the inverted position (backlobes toward ground). Comparison of the observed TA with that predicted using the antenna pattern employed in V2.0 indicated that this pattern was in error. An adjustment was made keeping the main lobe features of the existing model but adjusting the off-earth fraction ("spillover") to agree with the experiment [14]. Corresponding adjustments to the APC for V3.0 resulted in a significant improvement in the calibration at the warm and cold ends while keeping the good performance over ocean.

The performance in V3.0 with the adjusted "hybrid" antenna pattern is much improved. For example, agreement with SMOS over Dome-C in Antarctica is now better than 1 K (e.g., report

by F. Cabot at the meeting of the L-band Inter-Comparison Working Group, March 2014). In addition, Aquarius is now producing global maps of soil moisture which are in good agreement with SMOS. The soil moisture data are available from National Snow and Ice Data Center (NSIDC: http://nsidc.org/data/AQ2_SM) and example maps are available at the Aquarius outreach website: http://aquarius.umaine.edu. Also, the agreement at the cold end is much improved (see Fig. 15 and discussion in Section V).

C. Improvements in Roughness Correction

Several improvements have been made to the roughness correction. The effect of surface roughness (waves) is a potential major source of error in the retrieval [8], [17], [45], and the primary reason for including the scatterometer in the Aquarius instrumentation. The correction for roughness is made by developing an empirical relationship between the scatterometer radar cross section σ_o, and the difference in emissivity between the actual rough surface (observed) and an ideal flat surface (theory).

Among the changes made in V3.0 to the roughness correction were ([33], Sec. 3): 1) using winds derived from Aquarius data; 2) adding a temperature dependence to the isotropic term (i.e., the term not dependent on wind direction); and 3) including a small dependence on significant wave height.

The roughness correction uses the scatterometer radar cross section at vertical polarization (i.e., $\sigma_{\mathrm{o\_vv}}$) and also the local winds as input ([42] and Addenda). In V2.0, this relationship used NCEP winds. In V3.0, the NCEP winds were replaced by winds independently determined from the Aquarius radiometer and scatterometer observations. The Aquarius winds are derived by minimizing the residual between the measured scatterometer radar cross section for horizontal polarization $\sigma_{\mathrm{o\_hh}}$, and a model function for its dependence on wind speed and direction ([33], Sec. 2;[34]). There are two versions of this product, one which uses both $\sigma_{\mathrm{o\_hh}}$ and the radiometer brightness temperature $\mathrm{TB_H}$, and another which uses only $\sigma_{\mathrm{o\_hh}}$. The latter is used in certain cases when calibrated TB is not available.

D. Use both H and V Pol in Retrieval

In V2.0, only the radiometer data at vertical polarization, which is most sensitive to changes in salinity, were used in the salinity retrieval. In V3.0, the retrieval uses measurements at both vertical and horizontal polarizations. The radiative transport algorithm [28], [42] is used to transfer measurements at the spacecraft to the surface which are corrected for roughness (Section III-C) to produce a brightness temperature at the surface. Salinity is retrieved by minimizing the square difference between this measurement and the theoretical brightness temperature for a flat surface with the same temperature and incidence angle ([33], Sec. 4). That is by minimizing the difference

$$\chi^2 = \Big\{ \left[\mathrm{TB_{V\_meas}} - \mathrm{TB_{V\_theory}}\right]^2 / {\Sigma_\mathrm{V}}^2 + \left[\mathrm{TB_{H\_meas}} - \mathrm{TB_{H\_theory}}\right]^2 / {\Sigma_\mathrm{H}}^2 \Big\} \quad (1)$$

where $\mathrm{TB_{X\_theory}}$ is the value at polarization $\mathrm{X} = \{\mathrm{V}, \mathrm{H}\}$ obtained from the Fresnel reflectivity.

The residual in χ is also computed and reported in V3.0 as a quality index. For this purpose, χ is recomputed using the retrieved value of salinity in $\mathrm{TB_{X\_theory}}$ and the residual in Kelvin is reported as an indication of the quality of the solution. The parameters Σ_V and Σ_H in (1) are estimates based on global statistics and can be found in Section 4 of the Addendum III of the Aquarius ATBD [33].

E. Improved Correction for Radiometer Drift

As reported above (Section II-C1), the Aquarius radiometers have performed very well but a small drift in gain has been present since launch, which is removed as part of calibration. For this purpose, the drift is modeled in two parts: An exponential plus small residual deviations from the exponential. The exponential is computed once by fitting a simple exponential to the radiometer history. A fixed bias is removed as part of this fit so that the error on a global basis at time $= 0$ is zero. This part of the process has not changed in V3.0. However, the method for treating the residuals has been modified. The regional singular value decomposition adopted in Addendum II and used in V2.0 [38] has been abandoned for a simple 7-day average. In V3.0, the difference between observed and predicted TA, after removing the exponential component of drift, is averaged globally for every 7-day repeat cycle and removed in the form of bias in TA.

F. Flags and Masks

The radiometer flags and masks have been substantially revised for V3.0. Among the important changes are a series of masks that define data to be used for calibration (e.g., used to determine the radiometer drift correction discussed above). Certain areas suspected of contamination by RFI have been removed from the calibration data, and strict limits are applied to prevent contamination by land. These same flags are used but at a lower level of exclusion to mask data transferred from level 2 to level 3 products. A list of the flags can be found in Table I of the Aquarius level 2 product specification document. For additional details, see AQ-014-PS-0006 [30] and the notes below Table I in the Aquarius level 2 product specification document (available at the PO.DAAC).

G. SST Bias Correction

During the evaluation of the salinity retrieval algorithm, which is done by comparing the retrieved salinity with *in situ* measurements from Argo floats and from predictions using the HYCOM ocean model, a bias was found in V3.0 which appeared to correlate with sea surface temperature (SST) (e.g., [35]). This is illustrated in Figs. 7 and 8. The two panels in Fig. 7 show the difference between the retrieved salinity in V3.0 and that measured by Argo in geographic coordinates (top) and plotted as a function of latitude and time (bottom). The upper plot is the average for 1 year, and shows that, relative to Argo,

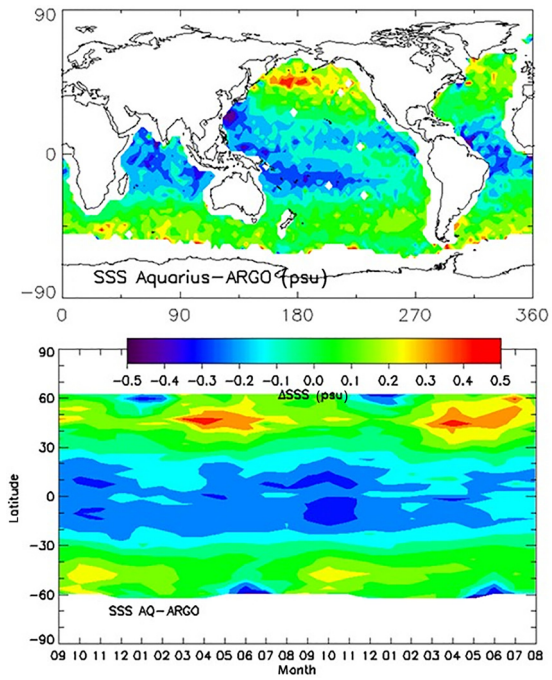

Fig. 7. Salinity retrieved by Aquarius minus salinity measured by Argo. The upper chart shows the data in geographical coordinates and the bottom figure shows the data as function of latitude (ordinate) and time (abscissa) for 2 years (September 2011–August, 2013).

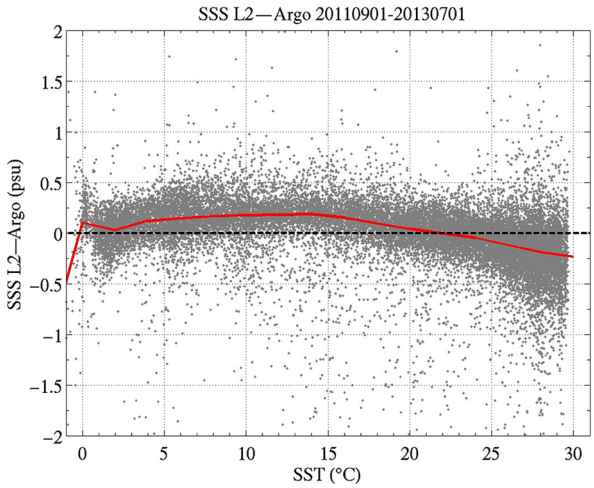

Fig. 8. Difference between salinity retrieved by Aquarius and salinity retrieved by Argo plotted as a function of SST. The gray dots represent the data (points of matchup between Argo and Aquarius averaged over $1^\circ \times 1^\circ$ bins monthly, and the red line shows the median at each temperature.

Aquarius is fresher in the low and mid-latitudes and saltier at high latitudes. The lower plot shows the full 3 years of measurements and shows that this trend is relatively independent of time with only minor seasonal variation. The latitudinal dependence suggests a correlation with SST which also tends to correlate with latitude. The dependence on SST is shown in Fig. 8 which plots the same data as function of SST. The ordinate is the salinity difference (Aquarius-Argo) and the abscissa is SST. The gray dots are the data (the difference in $1^\circ \times 1^\circ$ bins averaged monthly for the entire mission) and the red line is the median at each temperature. The tendency of the Aquarius salinity to be fresher in warm water and saltier in cold water is clearly evident from the median (red line).

At the present time, the cause for the correlation with SST has not been determined. Among the possibilities is the model for the dielectric constant. For example, using the Klein-Swift model [21] in place of the model currently employed in the Aquarius retrieval [32], [42] flattens the red curve for mid-range temperatures but increases the deviation for colder water [12]. But other temperature dependent terms in the forward algorithm, such as the temperature dependence of the term for atmospheric oxygen absorption or the temperature dependence in the surface roughness model, might also be responsible. In addition, systematic errors could exist in the auxiliary SST field (NOAA OI SST) that is used as input in the salinity retrieval algorithm.

Significant debate took place among the Aquarius Science team regarding what to do about the SST bias before releasing V3.0. A decision was made to issue two salinity products, a standard product and one with a correction for the SST bias. In order to keep the correction as transparent as possible, the decision was to adopt a single change, independent of location and applicable to the three radiometers

$$\Delta\mathrm{SSS} = -0.0019594 * \mathrm{T}^2 + 1.1257 * \mathrm{T} - 161.4934. \quad (2)$$

Users will find the standard product and a value of salinity with the correction available in the level 2 data at the PO.DAAC.

This simple correction does a reasonable job of removing the bias. This is illustrated in Fig. 9 which shows (left side) the same data as in Fig. 7 and on the right the data with the correction above applied. The relatively uniform colors in the two plots on the right suggest that a major improvement has been made. However, until the cause for the bias is known, care should be taken using this product.

IV. Examples

A. Average SSS

Aquarius is doing well and the changes made in V3.0 have improved the accuracy of the retrieval. For example, Fig. 10 shows the average salinity for the year September 2013 through August 2014. (Aquarius data-years are measured from when the instrument began operations in late August for 1 year, hence, September through August.) The maps show the features of the global salinity field one expects from climatology and also some surprises. For example, the map clearly shows the Atlantic Ocean saltier than the Pacific Ocean, and the separation of the salty maxima in the northern and southern hemispheres by the fresher water associated with rain in the Inter-Tropical Convergence Zone (ITCZ). In addition, one can see the saltier Arabian Sea where rain and runoff are limited compared to the much fresher Bay of Bengal and Indian Ocean where rain and runoff are significant. One of the pleasant surprises in the images is the detection of outflow from the major rivers. For example, the outflow from the Orinoco and Amazon rivers can be seen clearly off the northwestern coast of South America. Also, the enhanced fresh water at the north eastern edge of

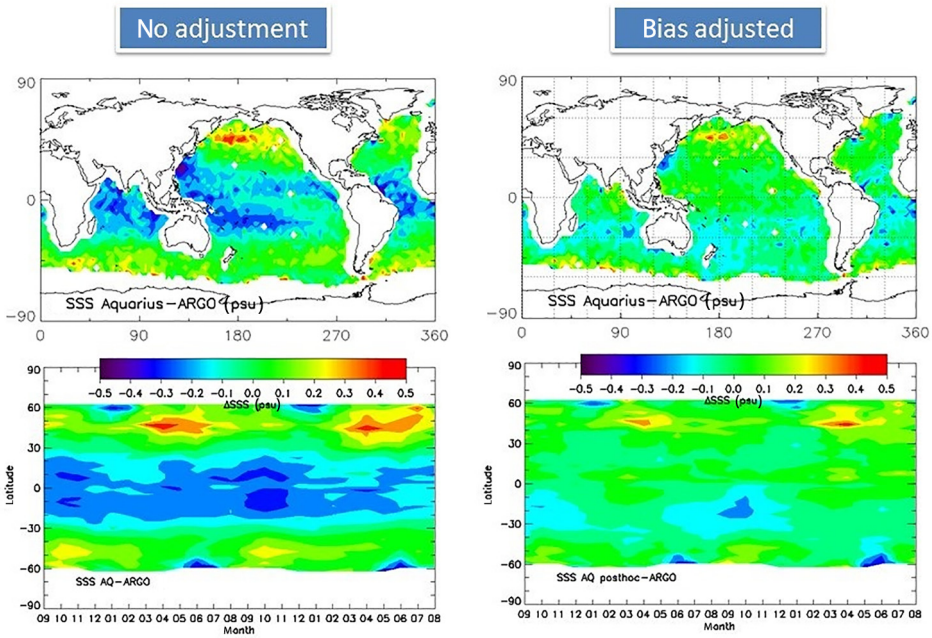

Fig. 9. Effect of the correction for the SST bias. (*Left*) The standard Aquarius L2 salinity retrieval. (*Right*) The same data after the bias correction (adjustment). The top figure shows the data in geographical coordinates and the bottom figures show the data as a function of latitude (ordinate) and time (abscissa). The uniform color of the figures on the right indicates the reduction in bias after the correction is made.

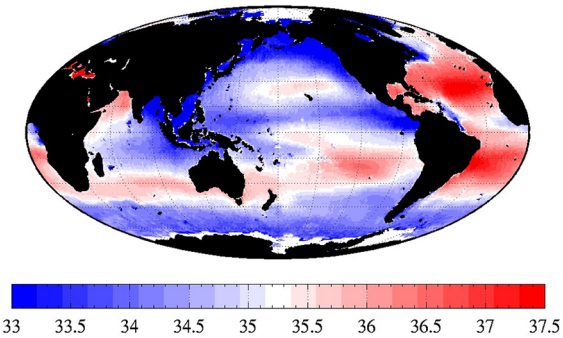

Fig. 10. Average global salinity field for the year September 2013–August 2014 retrieved by Aquarius using Version 3.0 of the salinity retrieval algorithm.

South America near Panama which is clearly evident in the map varies seasonally and periodically appears to split away from the main fresh band associated with the ITCZ. Examples and a movie showing the dynamic changes of the salinity field with season can be found at the Aquarius outreach website: http://aquarius.umaine.edu.

One of the goals of Aquarius is to study the interannual variations of the salinity field. Now, with three full years of data available, it is possible to begin to look at these changes. Fig. 11 shows the yearly change. The difference between the first 2 years of Aquarius data are shown on the left and the difference between years 2 and 3 is shown on the right. Some differences are to be expected such as the differences associated with changes in the mean outflow from the Orinoco and Amazon rivers, which is positive (red) between the years 1 and 2 and largely negative (blue) between years 2 and 3. However, other changes such as those associated with the ITCZ are less clearly explained; for example, the large blue arc extending from Indonesia almost to the tip of South America is clear in year 2–1 but almost disappears in year 3–2. There is also a significant change in the salinity of the water off the coast of Panama which becomes saltier (red) between years 2–1 and fresher between years 3–2. The purpose of this paper is not to propose an explanation for these changes but to point out the value of long term, global monitoring by Aquarius to document such changes and hopefully create the information for new insight.

B. Performance Metric

Two approaches have been used to quantitatively assess the performance of the Aquarius salinity retrieval. One is to compare the retrieved salinity with the *in situ* measurements of the Argo floats (see Argo). On the plus side of using Argo for comparison is the large number of floats (around 3000) covering a large portion of the oceans. On the negative side is that: 1) these are point measurements, each float providing one sample in (approximately) 10 days; 2) the floats do not sample at the surface (in order to prevent fouling of the sensor, the highest sample is usually about 5 m below the surface); and 3) the surfacing of the floats and the presence of an Aquarius footprint do not often coincide. Another approach is to compare with the predictions of the HYCOM model [7]. On the plus side, the model predicts near surface salinity in a consistent manner, and does so over the entire ocean. On the negative side, Aquarius uses the global average SSS from the HYCOM as part of calibration (to remove bias and correct for the radiometer drift). However, it does not use the local values in calibration, only the global average.

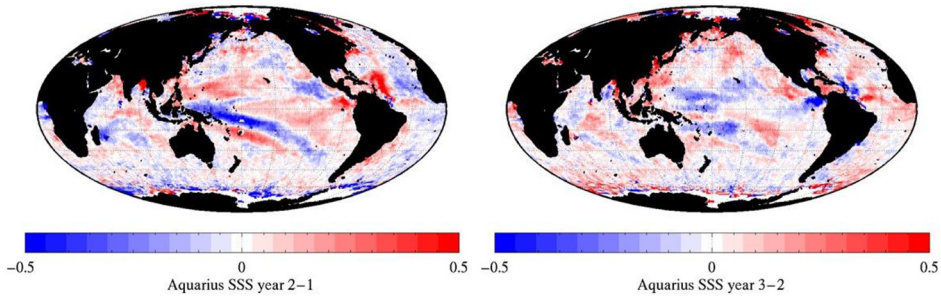

Fig. 11. Annual differences in the mean SSS field. (*Left*) Aquarius year 2 minus Aquarius year 1. (*Right*) Aquarius year 3 minus Aquarius year 2.

Difference between Aquarius and Argo Aquarius−Argo (psu)				
	Beam 1	Beam 2	Beam 3	All
Mean	−0.01	−0.02	−0.02	−0.03
STD	0.38	0.42	0.46	0.37

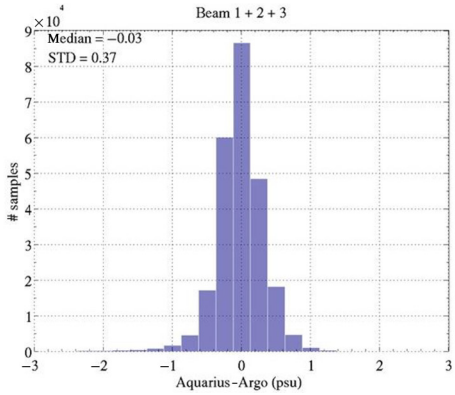

Fig. 12. Comparison of salinity retrieved by Aquarius and measured by Argo. The table presents the statistics of the match-ups by beam and for all beams. The histogram on the right shows the distribution of differences for all beams. The histograms for the individual beams are similar.

Fig. 12 illustrates the performance measured against the *in situ* Argo measurements. For this comparison, Aquarius footprints (beam center) which coincide with an Argo observation within 75 km and ± 3.5 days are considered to be a "match." These limits are consistent with the spatial and temporal resolution of Aquarius (100 km foot print and 7-day revisit time). But, even in the open ocean, a single point measurement may not adequately portray the salinity field within this time-space box. The match-ups are also done on the basis of the Aquarius fundamental 1.44 s retrievals (by comparison, the Nyquist time for the Aquarius footprint is on the order of 6–7 s). All 1.44 s samples which fall within the space–time window are averaged. Finally, level 2 masks are used (as opposed to the more restrictive masks for calibration data) with the exception that flag for cold water (temperature $< 5\ ^{\circ}\mathrm{C}$) and high winds ($\mathrm{wind} > 15\ \mathrm{m/s}$) is applied. The table in Fig. 12 lists the global mean and standard deviation of the difference between the Argo measurements and the Aquarius retrievals for each of the beams and for all three taken together. The figure is the histogram of the difference for the case of all three beams taken together. The individual histograms are similar.

Fig. 14 presents a breakdown of the global statistics in Fig. 12 by latitude. The table shows the standard deviation of the difference for all three beams ("all") and also separated into ascending and descending passes. The number in the last column is the number of Aquarius-Argo match-ups in each region. The red curve in the figure is a plot of the data in the column "all" in the table. The black curve is the mean value for "all" in each region. The black curve is another example of the SST bias that exists in the standard level 2 salinity retrieval in V3.0. The global mean is approximately zero (as shown in Fig. 12) but Fig. 13 shows that there are significant regional differences. The effect of the SST bias correction (2) is to flatten the black curve. The mean standard deviation is on the order of 0.2–0.3 psu for latitudes below about 30 N. The reason for the high values in the higher northern latitudes is not known, but among the possible causes are the decrease in sensitivity due to colder water and the possibility of undetected RFI (which is known to be strong in the Northern Atlantic Ocean near the coasts of the USA and Europe). Because of the potential for undetected RFI in areas near land where strong sources of RFI exist, Aquarius imposes "exclusion zones" in the mask defining data to be used for calibration. These masks have not been adopted here.

Figs. 12 and 13 probably represent a worst case comparison for Aquarius. They include all the issues associated with point samples, employ a liberal space–time window, use the weak set of flags and masks, use the oversampled data, and neglect rain. Since the Aquarius goal is 150 km maps with 0.2 psu accuracy on a monthly basis, an alternative is to first make monthly average maps of the Aquarius and ARGO data on a 150-km grid. Fig. 14 shows a comparison along these lines. In this case, the comparison also includes HYCOM. The data also have been filtered to remove observations in regions with rain. This is necessary to avoid bias due to freshwater stratification in the upper ocean layer where the Argo data are most likely to differ from Aquarius because they do not sample at the surface. In addition, the more stringent flags and masks associated with the calibration data have been used. The upper chart shows the standard deviation of the difference between the Aquarius retrieval and the observations of Argo and predictions of HYCOM.

	ALL	ASC	DSC	No.
50 – 60 N	0.55	0.70	0.62	3994
40 – 50 N	0.55	0.64	0.59	8798
30 – 40 N	0.51	0.41	0.72	15534
20 – 30 N	0.37	0.41	0.52	30383
10 – 20 N	0.27	0.34	0.32	22810
0 – 10 N	0.29	0.47	0.37	22775
0 – 10 S	0.29	0.36	0.39	22564
10 – 20 S	0.32	0.51	0.39	26494
20 - 30 S	0.25	0.36	0.31	24142
30 – 40 S	0.23	0.27	0.30	27340
40 – 50 S	0.29	0.38	0.39	31144
50 – 60 S	0.30	0.38	0.42	8931

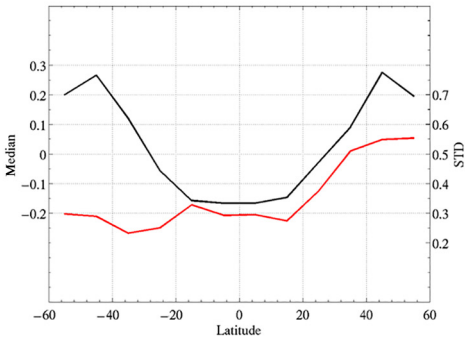

Fig. 13. Regional statistics of the comparison of Aquarius and Argo salinity. The figure shows the standard deviation as a function of latitude (red) and the mean bias (black). The standard deviation is listed in the table including a separation by ascending and descending orbit. The right-most column gives the number of match-ups in that region.

Differences between Aquarius, ARGO, and HYCOM (psu) 3° monthly averages			
	Aquarius–HYCOM	Aquarius–Argo	HYCOM – Argo
V3.0	0.29	0.31	0.25
SST bias adjusted	0.24	0.27	0.25

Triple location estimates of individual errors (psu) 3° monthly averages			
	Aquarius	HYCOM	Argo
V3.0	0.24	0.16	0.19
SST bias adjusted	0.18	0.16	0.19

Fig. 14. Comparison of Aquarius retrieved salinity with Argo and predicted by the HYCOM ocean model. (*Top*) The individual comparisons. (*Bottom*) Separation of errors by triple location.

This is shown both for the standard Aquarius product and the product with the SST bias adjustment. The lower chart shows an attempt to separate the errors inherent in each measurement. This was done assuming that error in Aquarius, Argo, and HYCOM are independent and solving for the error (triple location estimation). The three measurements are not strictly independent (Argo data are assimilated into the HYCOM model and Aquarius is debiased using the global average HYCOM salinity) but the coupling is weak and it is reasonable to assume that the errors are independent given the much different nature of the three data types. The results of the separation are shown in the bottom chart in Fig. 14 with and without the SST bias adjustment.

V. Discussion

Aquarius is doing well. Interannual differences are clearly evident in the salinity maps and the retrieval is approaching the goal of 0.2 psu. The retrieval is approaching the limit where issues associated with validation (i.e., representativeness of point samples, the presence of rain, the relationship of samples at 5 m to salinity at the surface, etc.) are as important as noise in the retrieval itself.

But more remains to be done to improve the retrieval. Among the on-going issues is continued improvement in the calibration over the full range of measurements (land, ocean, and sky). Soon there will be three L-band radiometers in space, SMOS, Aquarius, and SMAP, and the science user community will want to be able to combine these measurements (e.g., to combine Aquarius' accurate but low-resolution observations of SSS with the higher resolution of SMAP and SMOS in dynamic regions such as eddy formation along the Gulf Stream or near melting ice; or to include Aquarius measurements of soil moisture to augment those of SMOS and SMAP). To facilitate this, it is necessary to have Aquarius calibrated well over the full range of observations, as well as over the open ocean. In addition, new application has already begun to study the cryosphere that will need properly calibrated data TB at the warm end [4]–[6].

Version 3.0 made a major improvement in this direction, but work remains. The behavior when looking at cold sky illustrates this. Aquarius is periodically inverted to look away from the earth toward celestial space which is a very cold (3.5 K at the galactic poles) and stable scene. The brightness temperature of the celestial sky at L-band is relatively well known [11], [25] and easily modeled since the propagation path is essentially empty space. Fig. 15 shows the residual error (bias) remaining at several stages in the calibration history of Aquarius [13], [14]. The data points represent the residual for each of the three radiometer beams (1, 2, 3) and each polarization (vertical on the left and horizontal on the right). The data have been connected by straight lines to make them more visible. The red curves show the residual bias when looking at the cold sky as it existed in retrieval version 2.0. The green curve is the residual after modifing the forward algorithm to include the hybrid antenna pattern but using the Aquarius calibration as in V2.0. The blue curve is the current state of the calibration in Version 3.0 with the hybrid antenna pattern used in the forward model and the corresponding updated calibration. With the exception of vertical polarization in radiometer 3 (outer beam), the bias is less than 1 K and for most channels, substantially less. The reason why vertical polarization in radiometer 3 is so much out of line is one of the unknowns still to be resolved. It is especially perplexing since the channel

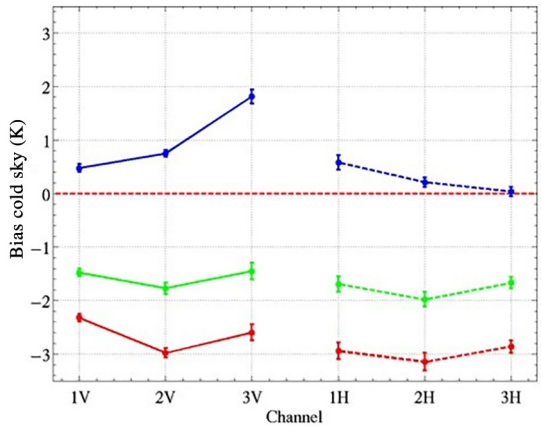

Fig. 15. Residual calibration bias when looking at cold sky: Version 2.0 (red), Version 2.0 with modified antenna pattern (green), Version 3.0 (blue). Vertical polarization (V) on the left and horizontal polarization (H) on the right for the three Aquarius radiometer channels.

for horizontal polarization for the same radiometer is almost perfect (i.e., essentially zero bias).

Another issue under review by the Aquarius team is the use of the HYCOM model for calibration. The HYCOM surface salinity field is used to remove a bias (a one-time adjustment) and to help correct for radiometer drift (Section II-C1). The long term goal is to eventually have an instrument-only calibration independent of the ocean [36] but until this is accomplished an ocean reference is needed. Debate continues within the Aquarius project over the advantages of using HYCOM or Argo floats. Currently, Argo floats are used for validation. The choice is not easy. HYCOM predicts a surface salinity; it "assimilates" *in situ* data such as from the Argo floats and it provides uniform global coverage. On the other hand, data from Argo represent truth (i.e., actual *in situ* measurements); but the data represent "point" measurements, the measurements do not reach the surface and they may not reflect the impact of rain. There are additional pros and cons, but in terms of establishing the global calibration bias, the differences are small.

Among the other issues that are currently under investigation are:

1) the source of the SST bias;
2) improvements in the RFI mitigation algorithm to correct missed detection of low level RFI in several regions in the North Atlantic and Western Pacific;
3) explanation for and removal of small residual interbeam bias;
4) assesment of the impact of rain and need for a correction;
5) a method to remove radiometer drift that is independent of the ocean model;
6) review of the ancillary data for SST.

Finally, the Aquarius prime mission ended November 30, 2014 (3 years of operations following completion of commissioning). The mission has been extended to the end of September 2015 (end of the US Government fiscal year) to align its schedule with other NASA missions seeking continuation. Assuming all is working well and new science continues to be produced, a proposal will be made by the project team to extend Aquarius for two more years (October 2015–September 2017). In addition to providing a longer record of salinity maps, an extension will provide a period of overlap with SMAP [15] and intercomparison of three L-band missions in space, Aquarius, SMAP, and SMOS [20].

Appendix

SAC-D Instruments

The CONAE contribution to the Aquarius/SAC-D observatory includes the spacecraft bus called "SAC-D" which is an abbreviation for Satélite de Aplicaciones Científicas (SAC) and the "D" indicates the fourth in this partnership with the United States, plus several instruments. Among the instruments on SAC-D are the MWR which operates at 36.5 and 23.8 GHz [3]. The MWR consists of twin 8-beam radiometers looking forward and aft of the spacecraft. The MWR is at the bottom of Fig. 1 (right side) where the reflectors for the two radiometers are labeled "MA" and the structure housing the feeds (eight for each radiometer) and electronics is labeled "MWR." The reflectors can be seen in their stowed position at the extreme bottom right in the photograph (labeled "4" in Fig. 2). The eight beams operate in pushbroom mode and are designed to cover the same swath as Aquarius (but oriented fore and aft of the real-time Aquarius footprint which is across-track). Among the goals of the MWR are to produce maps of winds, water vapor and rain over the ocean. Just to the left the MWR in the photograph and behind the two posts supporting antennas (labeled "5"), are two scanning cameras, the new infrared camera (NIRST) and the high sensitivity visible camera (HSC). The cameras support research on environmental monitoring such as measuring SST, monitoring light pollution, and other applications. To the left of the cameras and next to the Aquarius sun shield is an instrument built by the Italian Space Agency (ASI). This is also an L-band instrument called Radio Occultation Sounding of the Atmosphere (ROSA) and its goal is to monitor temperature and electron content of the ionosphere. It includes two antennas at the bottom Earth-facing side of the spacecraft (Fig. 1, right) and another antenna at the top (Fig. 1, left) labeled "RPOD." These antennas can be seen in their stowed position in the photograph (the earth-side antennas are the gray structure at the bottom and closest to the Aquarius Sun shield and labeled "6"). Finally, the SAC-D instruments include an instrument package for monitoring space debris and radiation called CARMEN 1 (ENvironment ChARacterization and Modeling) contributed by the French Space Agency (CNES). CARMEN consists of several small detectors distributed around the spacecraft bus and hidden by gray film in Fig. 2.

Papers describing the status of the SAC-D instruments and presenting examples of data from these instruments were presented at the Aquarius/SAC-D Science Team meetings in Buenos Aires (November 12–14, 2013) and in Seattle (November 11–14, 2014) and are available at the meeting websites: http://www.conae.gov.ar/prensa/Eventos/dia1.html and http://depts.washington.edu/uwconf/wordpress/aquarius. Among these reports is a description of progress

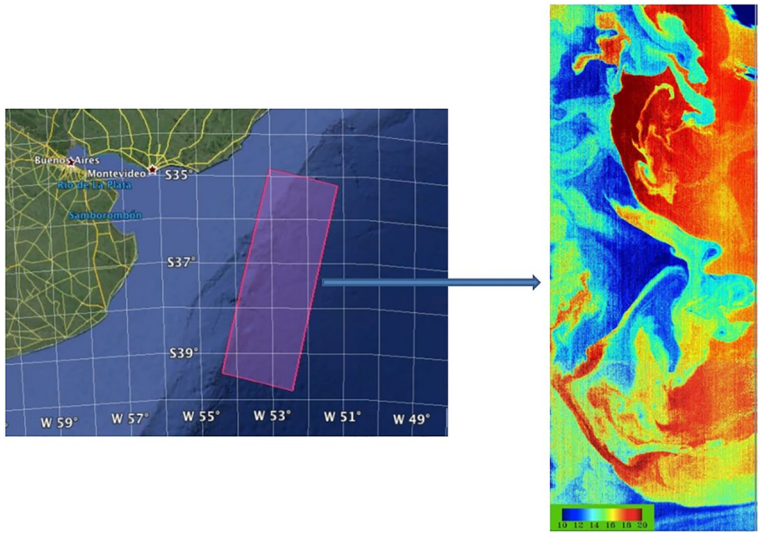

Fig. 16. Example of an image from the NIRST. (*Left*) A map showing the region of the image off the east coast of Argentina east of Buenos Aires. (*Right*) The color coded image of SST from NIRST. The scale is in degree Celsius (blue $= 10$ and red $= 20$).

made in the calibration of the NIRST using *in situ* measurements in Lake Tahoe. For example, Fig. 16 is an image from NIRST showing the temperature front associated with the confluence of the Brazil and Malvinas currents east of the coast of Argentina at the latitude of Buenos Aires. The HSC and DCS are operational and have been used to collect data to study ice dynamics in the Antarctic. For example, the HSC has been used to make visible surveys near the ice edge in the Weddell Sea and Antarctic Peninsula, and the DCS has been used to monitor ice movement in the Bahia del Diablo Glacier, Gourdon Glacier, and others. CARMEN has also been operating successfully and producing maps of radiation, but ROSA is still working on software issues. The MWR has been successfully calibrated and maps of rain, surface roughness, and winds have been produced which agree with other observations [2], [19]. Unfortunately, the MWR stopped working during the summer 2014. The root cause has not been established and at the date of this paper the instrument is not in science operating mode. The likely cause is a problem with the dc-to-dc converter in the power distribution network, but this has not been confirmed. However, the MWR has collected data for more than 2 years and calibrated level 1 data and level 2 products (rain and winds over the ocean) are available at the PO.DAAC: htttp://podaac.jpl.nasa.gov. Data from the SAC-D instruments are available at: http://www.conae.gov.ar/index.php/english/satellite-missions and at http://www.conae.gov.ar/index.php/espanol/catalogos/catdalogo-de-imagenes.

REFERENCES

[1] Argo [Online]. Available: http://www.argo.net/; also, D. Roemmich (Chair) *et al.*, *On the Design and Implementation of Argo—An Initial Plan for a Global Array of Profiling Floats* [Online]. Available: http://www.argo.ucsd.edu/argo-design.pdf

[2] S. Aslebagh, Y. Hejazin, W. L. Jones, C. May, and R. Gonzalez, "An oceanic rain flag for Aquarius," in *Proc. Oceans*, pp. 44–48, 2012. doi: 10.1109/OCEANS.2012.6404812.

[3] S. K. Biswas, L. Jones, D. Rocca, and J.-C. Gallio, "Aquarius/SAC-D microwave radiometer (MWR): Instrument description & brightness temperature calibration," in *Proc. IEEE Int. Geosci. Remote Sens. Symp. (IGARSS)*, 2012, pp. 2956–2959. doi:10.1109/IGARSS.2012.6350705.

[4] L. Brucker, E. P. Dinnat, G. Picard, and N. Champollion, "Effect of snow surface metamorphism on Aquarius L-band radiometer observations at Dome C, Antarctica," *IEEE Trans. Geosci. Remote Sens.*, vol. 52, no. 11, pp. 7408–7417, Nov. 2014.

[5] L. Brucker, E. P. Dinnat, and L. Koenig, "Weekly-gridded Aquarius L-band radiometer/scatterometer observations and salinity retrievals over the polar regions—Part 1: Product description," *Cryosphere*, vol. 8, no. 3, pp. 905–913, 2014.

[6] L. Brucker, E. P. Dinnat, and L. Koenig, "Weekly-gridded Aquarius L-band radiometer/scatterometer observations and salinity retrievals over the polar regions—Part 2: Initial product analysis," *Cryosphere*, vol. 8, no. 3, pp. 915–930, 2014.

[7] E. P. Chassignet *et al.*, "The HYCOM (HYbrid coordinate ocean model) data assimilative system," *J. Mar. Syst.*, vol. 65, no. 1–4, pp. 60–83, Mar. 2007.

[8] E. P. Dinnat, J. Boutin, G. Caudal, and J. Etcheto, "Issues concerning the sea emissivity modeling at L-band for retrieving surface salinity," *Radio Sci.*, vol. 38, no. 4, pp. 25-1–25-11, May 2003.

[9] E. P. Dinnat and D. M. Le Vine, "Impact of sun glint on salinity remote sensing: An example with the Aquarius radiometer," *IEEE Trans. Geosci. Remote Sens.*, vol. 46, no. 10, pp. 3137–3150, Oct. 2008.

[10] E. P. Dinnat, D. M. Le Vine, and S. Abraham, "L-band radiometry and reflection of the galaxy by a rough ocean surface," in *Proc. Microw. Radiometry Remote Sens. Environ. (MicroRad)*, Firenze, Italy, Mar. 11–14, 2008, pp. 1–4.

[11] E. P. Dinnat, D. M. Le Vine, S. Abraham, and N. Floury. (2010). *Map of Sky Background Brightness Temperature at L-Band* [Online]. Available: http://oceancolor.gsfc.nasa.gov/AQUARIUS/DinnatEtAl2010

[12] E. P. Dinnat, J. Boutin, X. Yin, and D. M. Le Vine, "Inter-comparison of SMOS and Aquarius sea surface salinity, and effects of the dielectric constant and vicarious calibration," in *Proc. Microw. Radiometry Remote Sens. Environ. (MicroRad)*, Pasadena, CA, USA, Mar. 2014, pp. 55–60.

[13] E. P. Dinnat, D. Le Vine, R. Bindlish, and J. Piepmeier, "Aquarius whole range calibration: Celestial Sky, ocean, and land targets," in *Proc. Microw. Radiometry Remote Sens. Environ. (MicroRad)*, Pasadena, CA, USA, Mar. 2014, pp. 192–196.

[14] E. P. Dinnat *et al.*, "Aquarius L-band radiometers cold sky calibration," 2015, submitted for publication.

[15] D. Entekhabi *et al.*, "The soil moisture active passive (SMAP) mission," *Proc. IEEE*, vol. 98, no. 5, pp. 704–716, May 2010.

[16] First image. (2011) *Aquarius First Image* [Online]. Available: http://www.nasa.gov/mission_pages/aquarius/news/aquarius20110922.html#.U0cuJFcmxU8

[17] J. Font, G. S. E. Lagerloef, D. M. Le Vine, A. Camps, and Q.-Z. Zanife, "The determination of surface salinity with the European SMOS space mission," *IEEE Trans. Geosci. Remote Sens.*, vol. 42, no. 10, pp. 2196–2205, Oct. 2004.
[18] A. G. Fore, S. H. Yueh, W. Tang, and A. K. Hayashi, "Aquarius wind speed products: Algorithms and validation," *IEEE Trans. Geosci. Remote Sens.*, vol. 52, no. 5, pp. 2920–2927, May 2013.
[19] Y. Hejazin, W. L. Jones, and S. El-Nimri, "A roughness correction algorithm for Aquarius," in *Proc. 13th Spec. Meeting Microw. Radiometry Remote Sens. Environ. (MicroRad)*, 2014, pp. 44–48. doi: 10.1109/MicroRad.2014.6878905.
[20] Y. H. Kerr *et al.*, "The SMOS mission: New tool for monitoring key elements of the global water 8 cycle," *Proc. IEEE*, vol. 98, no. 5, pp. 666–687, May 2010.
[21] L. Klein and C. Swift, "An improved model for the dielectric constant of seawater at microwave frequencies," *IEEE Trans. Antennas Propag.*, vol. 25, no. 1, pp. 104–111, Jan. 1977.
[22] G. S. E. Lagerloef *et al.*, "The Aquarius/SAC-D mission: Designed to meet the salinity remote sensing challenge," *Oceanography*, vol. 21, no. 1, pp. 69–81, Mar. 2008.
[23] G. Lagerloef and J. Font, "SMOS and Aquarius/SAC-D missions: The era of spaceborne salinity measurements is about to begin," in *Oceanography from Space*, V. Barale, J. F. R. Gower, and L. Alberotanza, Eds. New York, NY, USA: Springer, Feb. 2010, pp. 35–58.
[24] G. Lagerloef, T. Meissner, and F. Wentz, "Aquarius radiometer status," in *Proc. Microw. Radiometry Remote Sens. Environ. (MicroRad)*, 2014, pp. 226–227. doi: 10.1109/MicroRad.2014.6878945.
[25] D. M. L e Vine and S. Abraham, "Galactic noise and passive microwave remote sensing from space at L-band," *IEEE Trans. Geosci Remote Sens.*, vol. 42, no. 1, pp. 119–129, Jan. 2004.
[26] D. M. Le Vine, G. S. E. Lagerloef, R. Colomb, S. Yueh, and F. Pellerano, "Aquarius: An instrument to monitor sea surface salinity from space," *IEEE Trans. Geosci. Remote Sens.*, vol. 45, no. 7, pp. 2040–2050, Jul. 2007.
[27] D. M. Le Vine, G. S. E. Lagerloef, and S. E. Torrusio, "Aquarius and remote sensing of sea surface salinity from Space," *Proc. IEEE*, vol. 98, no. 5, pp. 688–703, May 2010.
[28] D. M. Le Vine, E. P. Dinnat, S. Abraham, P. de Matthaeis, and F. J. Wentz, "The Aquarius simulator and cold-sky calibration," *IEEE Trans. Geosci. Remote Sens.*, vol. 49, no. 9, pp. 3198–3210, Sep. 2011.
[29] D. M. Le Vine, E. P. Dinnat, G. S. E. Lagerloef, and P. de Matthaeis, "Aquarius: Status and recent results," *Radio Sci.*, vol. 49, no. 9, pp. 709–720, Sep. 2014.
[30] D. M. Le Vine and T. Meissner. (2014, Jun.). *Proposal for Flags and Masks* [Online]. Aquarius Project Document AQ-014-0006 [Online]. Available: http://podaac.jpl.nasa.gov/aquarius
[31] A. Martin, J. Boutin, D. Hauser, and E. Dinnat, "Active-passive synergy for interpreting ocean L-band emissivity: Results from the CAROLS airborne campaigns," *J. Geophys. Res. Oceans*, vol. 119, no. 8, pp. 4940–4957, Aug. 2014. ISSN: 2169-9275.
[32] T. Meissner and F. J. Wentz, "The complex dielectric constant of pure and sea water from microwave satellite observations," *IEEE Trans. Geosci. Remote Sens.*, vol. 42, no. 9, pp. 1836–1849, Sep. 2004.
[33] T. Meissner, F. Wentz, D. Le Vine, and J. Scott, "Addendum III to ATBD," Jet Propulsion Lab., Pasadena, CA, USA, Aquarius Rep. AQ-014-PS-0017, Jun. 2014 [Online]. Available: http://podaac-www.jpl.nasa.gov/aquarius
[34] T. Meissner, F. Wentz, and L. Ricciardulli, "The emission and scattering of L-band microwave radiation from rough ocean surfaces and wind speed measurements from Aquarius," *J. Geophys. Res. Oceans*, vol. 119, 2014, pp. 6499–6522. doi: 10.1002/2014JC009837.
[35] T. Meissner, F. Wentz, J. Scott, and K. Hilburn, "Upper ocean salinity stratification and rain freshening in the tropics observed from Aquarius," in *Proc. IEEE Int. Geosci. Remote Sens. Symp. (IGARSS'14)*, Quebec City, QC, Canada, Jul. 2014, pp. 5111–5114.
[36] S. Misra and S. T. Brown, "Towards a fully internally calibrated Aquarius brightness temperature measurement," in *Proc. Int. Geosci. Remote Sens. Symp. (IGARSS)*, Jul. 2014 [online]. Available: http://igarss2014.org/Papers/PublicSessionIndex3.asp?Sessionid=1228
[37] G. Neumann *et al.*, "Aquarius scatterometer calibration report," Jet Propulsion Lab., Pasadena, CA, USA, Mar. 15, 2012.
[38] J. Piepmeier *et al.*, "Aquarius radiometer post-launch calibration for product version 2," Jet Propulsion Lab., Pasadena, CA, USA, Aquarius Project Rep. AQ-014-PS-015, Feb. 2013 [Online]. Available: http://podaac-www.jpl.nasa.gov/aquarius
[39] M. Shimada, O. Isoguchi, T. Tadono, and K. Isono, "PALSAR radiometric and geometric calibration," *IEEE Trans. Geosci. Remote Sens.*, vol. 47, no. 12, part 1, pp. 3915–3932, Dec. 2009.
[40] J. van Zyl, Y. Kim, and S. Yueh, "Initial analysis of the polarization properties of one year of Aquarius data," Presented at IEEE Int. Geosci. Remote Sens. Symp., Melbourne, Australia, 2013.
[41] G. Vernieres *et al.*, "The impact of the assimilation of Aquarius sea surface salinity data in the GEOS ocean data assimilation system," *J. Geophys. Res.*, vol. 119, no. 10, pp. 6974–6987, Oct. 2014.
[42] F. J. Wentz and D. M. Le Vine, "Aquarius salinity retrieval algorithm, version 2: Algorithm theoretical basis document," Jet Propulsion Lab., Pasadena, CA, USA, RSS Tech. Rep. 082912, Aug. 2012 [Online] Available: http://podaac-www.jpl.nasa.gov/aquarius; Also see Addendum I, II and III.
[43] W. J. Wilson, A. Tanner, F. Pellerano, and K. Horgan, "Ultrastable radiometers for future sea surface salinity missions," Jet Propulsion Lab., Pasadena, CA, USA, Rep. D-31794, Apr. 2005.
[44] S. H. Yueh, "Estimates of Faraday rotation with passive microwave polarimetry for microwave remote sensing of earth surfaces," *IEEE Trans. Geosci. Remote Sens.*, vol. 38, no. 5, pp. 2434–2438, Sep. 2000.
[45] S. H. Yueh *et al.*, "Error sources and feasibility for microwave remote sensing of ocean surface salinity," *IEEE Trans. Geosci. Remote Sens.*, vol. 39, no. 5, pp. 1049–1059, May 2001.
[46] S. H. Yueh, S. J. Dinardo, A. G. Fore, and F. K. Li, "Passive and active L-band microwave observations and modeling of ocean surface winds," *IEEE Trans. Geosci. Remote Sens.*, vol. 48, no. 8, pp. 3087–3100, Aug. 2010.
[47] S. Yueh *et al.*, "Aquarius post launch instrument calibration and validation plan," Jet Propulsion Lab., Pasadena, CA, USA, Rep., JPL-D52714, Jun. 2011.
[48] S. H. Yueh *et al.*, "L-band passive and active microwave geophysical model functions of ocean surface winds and applications to Aquarius retrieval," *IEEE Trans. Geosci. Remote Sens.*, vol. 51, no. 9, pp. 4619–4632, Sep. 2013.

David M. Le Vine (F'95) received the Ph.D. degree in electrical engineering from the University of Michigan, Ann Arbor, MI, USA.

His teaching experience includes the Department of Electrical Engineering, University of Maryland, College Park, MD, USA, and the Adjunct Faculty at the George Washington University, Washington, DC, USA. He is currently the Deputy Principle Investigator for Aquarius, a NASA Earth System Science Pathfinder (ESSP) mission to measure sea surface salinity. He also is a Member of the Science Team for NASA's Soil Moisture Active Passive (SMAP) mission and the Quality Working Group supporting ESA's Soil Moisture and Ocean Salinity (SMOS) mission. He works in the Earth Sciences Division at NASA's Goddard Space Flight Center, where he does research to develop techniques for microwave remote sensing of the environment from space. His research interests include passive remote sensing at the long wavelength end of the microwave spectrum (e.g., L-band) with applications to remote sensing of soil moisture and sea surface salinity.

Dr. Le Vine is a member of the Geoscience and Remote Sensing Society (GRSS) and Antennas and Propagation Society. He is currently a member of the GRSS AdCom and also a member of the International Union of Radio Science (URSI) and the American Geophysical Union.

Emmanuel P. Dinnat (M'12) received the Master's degree in instrumental methods in astrophysics and spatial applications and the Ph.D. degree in computer science, telecommunications, and electronics from the University Pierre and Marie Curie, Paris, France, in 1999 and 2003, respectively.

He is currently a Research Scientist with the Center of Excellence in Earth Systems Modeling and Observations (CEESMO), Chapman University, Orange, CA, USA, and the Cryospheric Sciences Laboratory, NASA Goddard Space Flight Center (GSFC), Greenbelt, MD, USA. Between 2003 and 2005, he was a Research Fellow with the European Space Agency (ESA) European Space Research and Technical Centre (ESTEC), Nordwijk, The Netherlands, where he worked on the Soil Moisture and Ocean Salinity (SMOS) mission. He joined the NASA GSFC in 2005 to work on the Aquarius instrument under the NASA Postdoctoral Program, first with the National Research Council (NRC) and then with the Oak Ridge Associated Universities (ORAU) from 2006 to 2007. He was an Assistant Research Scientist with the Goddard Earth Sciences and Technology Center/University of Maryland Baltimore County (GEST/UMBC) between 2007 and 2010. His research interests include active and passive

microwave remote sensing, sea surface salinity, scattering from rough surfaces, atmospheric radiative transfer, and numerical simulation, high latitude oceanography, and the interactions between the cryosphere and oceans.

Dr. Dinnat is a member of the American Geophysical Union (AGU) and the Institute of Electrical and Electronics Engineers (IEEE). He was the receipient of the GSFC's Hydrospheric and Biospheric Sciences Laboratory Peer Review Awards for Outstanding Postdoc/Research Associate and Outstanding Publication in 2006 and 2008, respectively, and two NASA Group Achievement Awards as a member of the Aquarius commissioning and calibration/validation teams in 2012 and 2013, respectively.

Thomas Meissner (M'02–SM'13) received the B.S. degree in physics from the University of Erlangen-Nürnberg, Erlangen, Germany, in 1983, the M.S. (Diploma) degree in physics from the University of Bonn, Bonn, Germany, in 1987, and the Ph.D. degree in theoretical physics from the University of Bochum, Germany, in 1991.

Between 1992 and 1998, he conducted Postdoctoral Research at the University of Washington, Seattle, WA, USA, the University of South Carolina, Columbia, SC, USA, and Carnegie Mellon University, Pittsburgh, PA, USA, in Theoretical Nuclear and Particle Physics. In 1998, he joined Remote Sensing Systems (RSS), Santa Rosa, CA, USA. Since then, he has been working on the development and refinement of radiative transfer models, calibration, validation and ocean retrieval algorithms for various microwave instruments (SSM/I, TMI, AMSR-E, WindSat, CMIS, SSMIS, GMI, Aquarius).

Dr. Meissner has been serving on the Review Panel for the National Academies' Committee on Radio Frequencies (CORF). As a member of the Aquarius Launch, Early Orbit Operations, and Commissioning Team, he has been recognized with the NASA Group Achievement Award in 2012. In 2013, he received the IEEE TRANSACTIONS ON GEOSCIENCE AND REMOTE SENSING Prized Paper Award for the paper describing the RSS ocean radiative transfer model.

Simon H. Yueh (F'09) received the Ph.D. degree in electrical engineering from Massachusetts Institute of Technology, Cambridge, MA, USA, in 1991.

He was a Postdoctoral Research Associate with the Massachusetts Institute of Technology from February to August 1991. In September 1991, he joined the Radar Science and Engineering Section, Jet Propulsion Laboratory (JPL), Pasadena, CA, USA. He was the Supervisor of Radar System Engineering and Algorithm Development Group from 2002 to 2007. He was the Deputy Manager of Climate, Oceans, and Solid Earth Section from 2007 to 2009, and the Section Manager from 2009 to 2013. He served as the Project Scientist of the National Aeronautics and Space Administration (NASA) Aquarius mission from January 2012 to September 2013, the Deputy Project Scientist of NASA Soil Moisture Active Passive Mission from January 2013 to September 2013, and the SMAP Project Scientist since October 2013. He has been the Principal/Co-Investigator of numerous NASA and DOD research projects on remote sensing of soil moisture, terrestrial snow, ocean salinity, and ocean wind. He has authored 4 book chapters and more than 150 publications and presentations.

Dr. Yueh is an Associate Editor of IEEE TRANSACTIONS ON GEOSCIENCE AND REMOTE SENSING. He was the recipient of the IEEE GRSS Transaction Prize Paper Award in 1995, 2002, 2010, and 2014, the 2000 Best Paper Award in the IEEE International Geoscience and Remote Symposium, the JPL Lew Allen Award in 1998 and Ed Stone Award in 2003, and the NASA Exceptional Technology Achievement Medal in 2014.

Frank J. Wentz received the B.S. and M.S. degrees in physics from Massachusetts Institute of Technology, Cambridge, MA, USA, in 1969 and 1971, respectively.

In 1974, he established Remote Sensing Systems, a research company specializing in satellite microwave remote sensing of the Earth. As a member of NASA's SeaSat Experiment Team (1978–1982), he pioneered the development of physically based retrieval methods for microwave scatterometers and radiometers. Starting in 1987, he took the lead on providing the worldwide research community with high-quality ocean products derived from satellite microwave imagers (SSM/I). As the President of RSS, he oversees the production and validation of climate-quality satellite products. He is currently a member of NASA Advanced Microwave Scanning Radiometer (AMSR) Team, NASA Ocean Vector Wind Science (OVWST) Team, the Aquarius Launch, Early Orbit Operations and Commissioning Team, and NASA MEaSUREs DISCOVER Project. He has served on many NASA review panels, the National Research Council's Earth Studies Board, and the National Research Council's Panel on Reconciling Temperature Observations. He is a Lead Author for *CCSP Synthesis and Assessment Product on Temperature Trends in the Lower Atmosphere.* He is currently working on scatterometer/radiometer combinations, satellite-derived decadal time series of atmospheric moisture and temperature, the measurement of sea-surface temperature through clouds, and advanced microwave sensor designs for climatological studies.

Dr. Wentz is a Fellow of the American Geophysical Union (2013), the American Meteorological Society (2015), and the American Association for the Advancement of Science (2015). He received the IEEE Transactions on Geoscience and Remote Sensing Prized Paper Award for the paper describing the RSS ocean radiative transfer model in 2013. As a member of the Aquarius Launch, Early Orbit Operations and Commissioning Team, he was recognized with the NASA Group Achievement Award in 2012. In 2015, he received the distinguished Verner E. Suomi Award for "pioneering, painstaking work to accurately retrieve geophysical parameters from satellite microwave instruments and using these measurements to elucidate climate trends."

Sandra E. Torrusio received the Ph.D. degree in natural sciences from the National University of La Plata, La Plata, Argentina.

She is an expert in applied to natural resources and environmental topics. She has participated in several international courses of remote sensing and applications (Italy, France, Sweden, Japan, Chile) and she has authored more than 20 publications in national and international journals. She has more than 30 presentations in national and international meetings, and is a reviewer in several journals. She is the Thesis Director and Evaluator and Member of Assessor Committees at local universities. She is Professor of Remote Sensing & GIS, Faculty of Natural Sciences (undergraduate and graduate level), at the National University of La Plata, UNLP, and she conducted postgraduate training courses. She is the Principal Investigator of the SAC-C and SAC-D Satellite Missions and Co-Investigator of SABIA-Mar, satellite mission of the Argentine space agency, Comision Nacional de Actividades Espaciales (CONAE).

G. Lagerloef received the Ph.D. degree in physical oceanography from the University of Washington, Seattle, WA, USA, in 1984.

He specializes in ocean circulation and climate dynamics with special emphasis in developing new applications for satellite remote sensing. He is currently serves as Principal Investigator of the NASA Aquarius Mission, which was launched in 2011 to study the interactions between the Earth's water cycle, ocean circulation, and climate. He has authored over 60 publications and presentations. He has served on numerous scientific teams and working groups over the past 15 years, a sampling of which include the Salinity Sea Ice Working Group (Chair), Satellite Altimeter Requirements for Climate Research Working Group (Co-Chair), NRC Committee on Earth Gravity Measurements from Space, the AMS Committee on Sea Air Interaction, and on NASA Science Working Teams for Topex/Poseiden/Jason missions, Ocean Vector Winds, and the Tropical Rainfall Measurement Mission. Prior to founding Earth and Space Research in 1995, he worked with the Science Applications International Corporation; the Joint Oceanographic Institutions, Detail to NASA. He was an NOAA Commissioned Officer and served in the U.S. Coast Guard. He is a member of several professional associations, learned, and technical societies.

Dr. Lagerloef has been a Guest Editor for the prestigious *Journal of Geophysical Research—Oceans*.